Biosensors and Bioelectronics 60 (2014) 1–7

Contents lists available at ScienceDirect

Biosensors and Bioelectronics

journal homepage: www.elsevier.com/locate/bios

A high sensitive biosensor based on FePt/CNTs nanocomposite /*N*-(4-hydroxyphenyl)-3,5-dinitrobenzamide modified carbon paste electrode for simultaneous determination of glutathione and piroxicam

Hassan Karimi-Maleh [a,*], Fahimeh Tahernejad-Javazmi [a], Ali A. Ensafi [b], Reza Moradi [c], Shadpour Mallakpour [b], Hadi Beitollahi [d]

[a] Department of Chemistry, Graduate University of Advanced Technology, Kerman, Iran
[b] Department of Chemistry, Isfahan University of Technology, Isfahan, Iran
[c] Department of Physics, Qaemshahr Branch, Islamic Azad University, Qaemshahr, Iran
[d] Environment Department, Institute of Science and High Technology and Environmental Sciences, Graduate University of Advanced Technology, Kerman, Iran

ARTICLE INFO

Article history:
Received 8 January 2014
Received in revised form
11 March 2014
Accepted 26 March 2014
Available online 2 April 2014

Keywords:
Glutathione
Piroxicam
Biosensor
Voltammetry
FePt/CNTs

ABSTRACT

This study describes the development, electrochemical characterization and utilization of novel modified *N*-(4-hydroxyphenyl)-3,5-dinitrobenzamide-FePt/CNTs carbon paste electrode for the electrocatalytic determination of glutathione (GSH) in the presence of piroxicam (PXM) for the first time. The synthesized nanocomposite was characterized with different methods such as TEM and XRD. The modified electrode exhibited a potent and persistent electron mediating behavior followed by well-separated oxidation peaks of GSH and PXM. The peak currents were linearly dependent on GSH and PXM concentrations in the range of 0.004–340 and 0.5–550 μmol L^{-1}, with detection limits of 1.0 nmol L^{-1} and 0.1 μmol L^{-1}, respectively. The modified electrode was successfully used for the determination of the analytes in real samples with satisfactory results.

1. Introduction

Glutathione is the most important molecule that need to stay healthy and prevent aging, cancer, heart disease, dementia and more, and necessary to treat everything from autism to Alzheimer's disease. The role of glutathione in the human metabolism includes protection against oxidative stress and detoxification of xenobiotics. In addition, it plays an essential role in many important biological phenomena, including the synthesis of proteins and DNA and protection of cells against free radicals (Ensafi et al., 2008). Studies have shown that the total GSH present in cells may be either free or bound to proteins. The amount of free GSH in blood is indicative of cell protection against oxidative and free radical-mediated cell injury. In addition, GSH levels in blood samples help in diagnosis of c-glutamyl cycle disorders. Its precise determination is, therefore, of utmost importance for diagnostic purposes (Ensafi et al., 2012; Keyvanfard et al., 2013). The determination of GSH has been carried out with various detection techniques such as titrimetry (Nagendra et al., 2002), spectrophotometry (Kamata, et al., 1995; Raggi et al., 1991), spectrofluorimetry (Liang et al., 2002; Zhang et al., 2005; Kandar et al., 2007), high performance liquid chromatography (HPLC) (Katrusiak et al., 2001; Xu et al., 2002), capillary zone electrophoresis (Causse et al., 2000), proton nuclear magnetic resonance (1H NMR) (Rabenstein et al., 1985), enzymatic method (Satoh et al., 1988), flow injection analysis (Ensafi et al., 2008) and electrochemical methods (Raoof et al., 2009a, 2009b; Ensafi et al., 2010).

Piroxicam is a non-steroidal anti inflammatory drug (NSAIDs) with analgesic and anti-pyretic activities (Bavili Tabrizi, 2007). Piroxicam exhibited a rapid and effective response in the treatment of many diseases such as rheumatoid arthritis, osteoarthritis, ankylosing spondylitis, gout juvenile rheumatoid arthritis, musculoskeletal disorders, postpartum pain and sport injuries. The most serious reported side effects are gastrointestinal effects, such as ulcer, bleeding ulcers, etc (Damiani et al., 1998).

Also, PXM as NSAIDs can be effective on the biological compounds that presence in the brain especially on concentration of glutathione (Damiani et al., 1998). So, these facts let us assume that piroxicam produce toxic events that are different according to the brain ((El-Sherbiny et al., 2009).

Electrochemical biosensors have been the subject of basic as well as applied research for nearly fifty years. Studies show that

* Corresponding author. Tel.: +98 911 2540112 (mob.); fax: +983412121018.
E-mail address: h.karimi.maleh@gmail.com (H. Karimi-Maleh).

http://dx.doi.org/10.1016/j.bios.2014.03.055
0956-5663/

electrochemical biosensors modified with nanomaterials can be improve electrical signal for important biological compounds with high overpotential and low intensity (Micheli et al., 1993; Ensafi et al., 2011a,2011b,2011c; Sanghavi and Srivastava, 2011, 2010; Sanghavi et al., 2013; Yola et al., 2013). So, much attention has been done for preparation of high selective and sensitive electrochemical biosensors for analysis of biological compounds in biological and pharmaceutical samples such as urine, blood and tablet (Yola et al., 2012; Gupta et al., 2014, 2005, 2013).

According to the above points, it is very important to create suitable conditions for the simultaneous analysis of GSH and PXM in biological samples. However, to best of our knowledge, there is no report on the voltammetric determination of GSH and PXM simultaneously; using modified electrodes. Therefore, in continuation of our studies on the preparation of chemically modified electrodes (Karimi-Maleh et al., 2013; Elyasi et al., 2013; Moradi et al., 2013; Ensafi et al., 2011a,2011b,2011c; Sanati et al., 2014), a novel *N*-(4-hydroxyphenyl)-3,5-dinitrobenzamide-FePt/CNTs carbon paste electrode (NHPDA/FePt/CNTs/CPE) for the voltammetric determination of GSH was investigated using square wave voltammetry. We have also evaluated the analytical performance of the modified electrode for quantification of GSH in the presence of PXM in some real samples.

2. Experimental

2.1. Synthesis of FePt/CNTs nanocomposite

Before introducing the FePt particles onto the surface of the CNTs, the CNTs were treated by boiling the as-received CNTs in mixture of HNO_3:H_2SO_4 for 4 h, rinse with distilled water, dried and ground.

FePt nanoparticles supported on multi-walled carbon nanotubes obtained by mixing stoichiometric of purified MWCNTs, Fe $(acac)_3$ (0.5 mmol), $Pt(acac)_2$ (0.5 mmol) and 1,2 Hexadecanediol (5 mmol) in 40 mL phenylether at room temperature under a flow of N_2 atmosphere, and then the solution was heated at 100 °C for 20 min. Reduction of Fe and Pt atoms in the presence of 1,2 Hexadeconediol have been obtained until starting the reduction of Fe and Pt salts and nucleation of FePt nanoparticles. Afterward the solution was heated to 260 °C for 90 min during the reflux process. After completion of reaction, the black product solution was cooled to room temperature under flow of N_2 atmosphere. Then the product was rinsed with ethanol and hexane solution for 3 times and dried in 200 °C under Ar atmosphere.

2.2. Chemicals

All chemicals used were of analytical reagent grade purchased from Merck (Darmstadt, Germany) unless otherwise stated. Doubly distilled water was used throughout.

A 1.0×10^{-2} mol L^{-1} GSH solution was prepared daily by dissolving 0.30 g glutathione in water and dilution the solution to 100 mL with water in a 100-mL volumetric flask. The solution was kept in a refrigerator at 4 °C and in dark. More dilute solutions were prepared by serial dilution with water.

A 1.0×10^{-3} mol L^{-1} PXM solution was prepared daily by dissolving 0.033 g PXM in methanol–water (1:1 v/v) and the solution was diluted to 100-mL with water in a 100-mL volumetric flask. The solution was kept in a refrigerator at 4 °C in dark. More dilute solutions were prepared by serial dilution with water.

Phosphate buffer (sodium dihydrogen phosphate and disodum monohydrogen phophate plus sodium hydroxide, 0.1 mol L^{-1}) solutions (PBS) with different pH values were used.

2.3. Apparatus

Square wave voltammetry (SWV), cyclic voltammetry, electrochemical impedance spectroscopy (EIS) and chronoamperomtry were performed in an electroanalytical system, Autolab PGSTAT 12N, potentiostat/galvanostat connected to a three-electrode cell, Metrohm Model 663 VA stand linked with a computer (Pentium IV, 1200 MHz) and with Autolab software. The system was run on a PC using GPES and FRA 4.9 software. For impedance measurements, a frequency range of 100 kHz–0.1 Hz was employed. The AC voltage amplitude was 5 mV, and the equilibrium time was 30 min. A conventional three-electrode cell assembly consisting of a platinum wire as an auxiliary electrode and an $Ag/AgCl/KCl_{sat}$ electrode as a reference electrode was used. The working electrode was either a carbon paste electrode (CPE), FePt/CNTs/CPE, NHPDA/FePt/CNTs/CPE or NHPDA/CPE.

2.4. Preparation of the modified electrode

30.0 mg of NHPDA was hand mixed with 870 mg of graphite powder and 100 mg of FePt/CNTs in a mortar and pestle. Using a syringe, 0.55 g of paraffin was added to the mixture and mixed well for 45 min until a uniformly wetted paste was obtained. The paste was then packed into a glass tube. Electrical contact was made by pushing a copper wire down the glass tube into the back of the mixture. When necessary, a new surface was obtained by pushing an excess of the paste out of the tube and polishing it on a weighing paper. The unmodified carbon paste electrode was prepared in the same way without adding mediator and NHPDA/FePt/CNTs/CPE to the mixture.

2.5. Preparation of real samples

Human whole blood was obtained from the Kerman Health Center and erythrocytes were separated from whole blood by removing the plasma. Human whole blood (2.0 mL) was first centrifuged for 10 min at 3000 rpm. The supernatant (plasma) was discarded and the rest was mixed with 5 mL of 0.9% NaCl solution. The solution was centrifuged for another 10 min at 4000 rpm and the supernatant (diluted plasma) was again discarded. The washing procedure with NaCl solution was repeated three times in order to remove the plasma almost completely.

The erythrocyte pellets were hemolysed with water (1:1, v/v). For protein precipitation, the hemolysate was mixed with 5-sulfosalysilic acid (10%, m/v) in the ratio of 2:1 (v/v). This mixture was centrifuged in the same condition described above. Then, the supernatant was divided to two parts, one for spectrophotometric determination and another for the proposed electrochemical method. For spectrophotometric measurements of the Ellman, a reference method (Ellman, 1959) was performed which is based on the reaction of glutathione and DTNB (Ellman's reagent), generating 2-nitro-5-mercapto-benzoic acid. The absorbance was monitored spectrophotometrically at 412 nm.

The urine samples were stored in a refrigerator immediately after collection. Ten milliliters of the sample was centrifuged for 30 min at 2500 rpm. The supernatant was filtered using a 0.45 μm filter and then diluted 10-times with PBS (pH 6.0). The solution was transferred into the voltammetric cell to be analyzed without any further pretreatment. The standard addition method was used for the determination of GSH in real samples.

The tablet solution was prepared by completely grinding and homogenizing seven tablets of GSH, labeled 100 mg per tablet (Chongqing Yaoyou Pharmaceutical Co., Ltd.). Then, 10 mg of each tablet powder was accurately weighed and dissolved in 100 mL water by ultrasonication. After mixing completely, the mixture was filtered on an ordinary filter paper, 10 mL of which was

subsequently transferred into a 100-mL volumetric flask and diluted to the mark with water. Then, 1.0 mL of the solution plus 4.5 mL of the buffer (pH 7.0) was used for analysis using the standard addition method.

3. Results and discussion

3.1. Nanostructures characterization

The morphology of the as-grown nanostructures was characterized by TEM. Fig. 1A shows a typical TEM image of FePt/CNTs composite. The dark spots correspond to FePt nanoparticles, which were only deposited on sidewalls of MWCNTs. Bimetallic FePt NPs with near spherical shapes, were synthesized onto MWCNTs. Fig. 1B is the histogram of FePt nanoparticles size distribution based on log-normal fitting. Histogram graph shows that the particles have a single size with an average diameter ($<d>$) about 2.96 nm and standard deviation (σ) of about 0.75, indicate narrow size distribution ($\sigma/<d>$) of 0.25. Also, comparing of TEM images of CNTs (Fig. 1C) and FePt/CNTs confirm presence of FePt in synthesis of FePt/CNTs.

PtFe nanoalloy was analyzed by XRD analyses. The diffraction angles at 2θ=40.0, 46.1 and 68.4 (Fig. 1D), can be assigned to (1 1 1), (2 0 0) and (2 2 0) planes of FePt nanoalloy. The peak at 26.1 can be nicely indexed to the (0 0 2) plane of MWNTs as marked. The broad peaks in the XRD patterns indicate that the FePt nanoalloy is small. The mean particle size of FePt nanoalloy calculated by the Scherrer equation is about 2.5 nm.

3.2. Electrochemical investigation

As NHPDA is insoluble in an aqueous solution, it can be easily incorporated into a carbon paste without concern for its leaching from the electrode surface. This fabrication process yields a stable and chemically-modified electrode. The cyclic voltammogram exhibits an anodic peak at the forward scan of the potential related to the oxidation of the NHPDA to 1,2-benzoquinone form. In the reverse scan of the potential, a cathodic peak appears related to the reduction of 1,2-benzoquinone form, to NHPDA (Fig. 2 curve *a*). A pair of quasi-reversible peaks are observed at E_{pa}=0.42 V and E_{pc}=0.23 V vs. Ag/AgCl. The half-wave potential ($E_{1/2}$) was 0.32 V vs. Ag/AgCl and ΔE_p ($E_{pa}-E_{pc}$) was 0.16 V. The electrode process was quasi-reversible, with ΔE_p, greater than the expected value (59/n mV) for a reversible system. The plot of the anodic peak current was linearly dependent on $\upsilon^{1/2}$ for all scan rates. This behavior indicates that the nature of the redox process is diffusion controlled.

The electrocatalytic behaviors of NHPDA/FePt/CNTs/CPE in the buffer solution (pH 7.0) were studied. Fig. 2 shows the cyclic voltammetric responses behavior of NHPDA/FePt/CNTs/CPE (curve *a*) in a solution without GSH, and of NHPDA/CPE (curve *b*), NHPDA/FePt/CNTs/CPE (curve *c*), FePt/CNTs/CPE (curve *d*) and CPE (curve *e*) in the presence of 300.0 μmol L^{-1} GSH. As shown, the anodic peak potential for GSH oxidation at NHPDA/FePt/CNTs/CPE (curve *c*) and

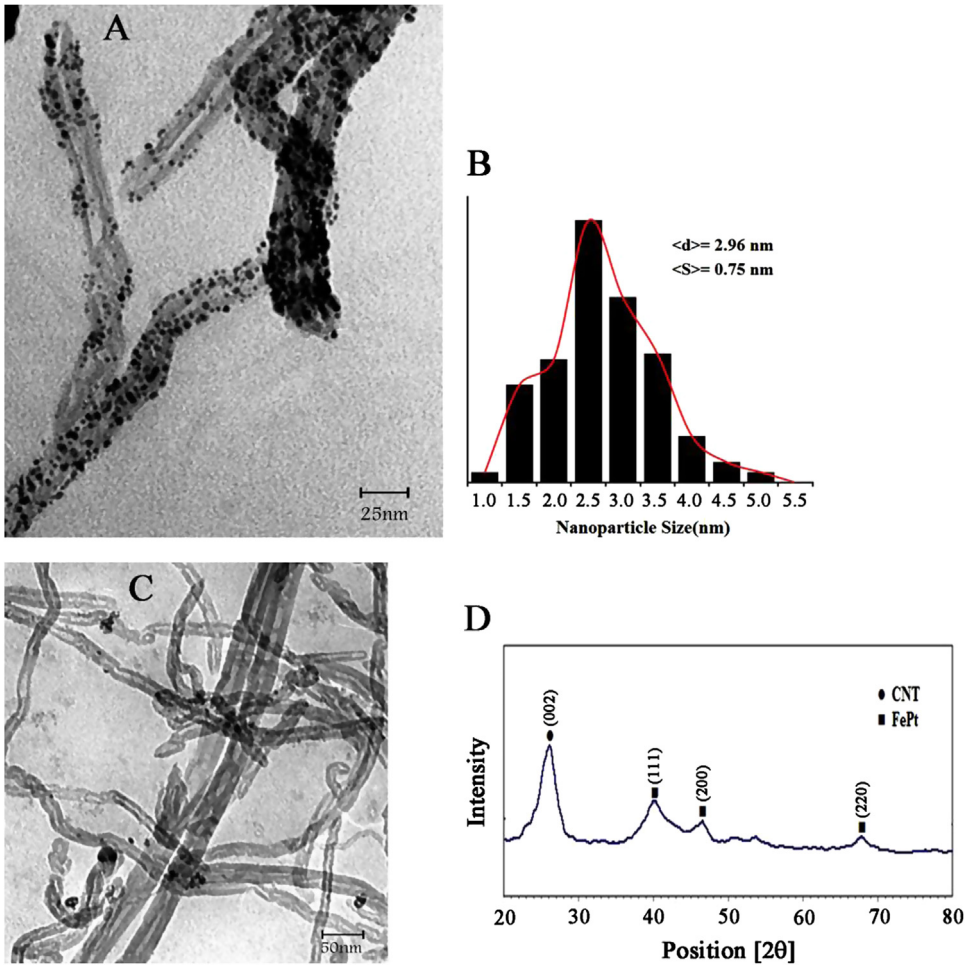

Fig.1. (A) TEM image of FePt nanoparticles deposited on the sidewalls of MWCNTs. (B) Histogram of size distribution of FePt nanoparticles. (C) TEM image of MWCNTs and (D) XRD patterns of as-synthesized FePt/CNTs nanocomposite.

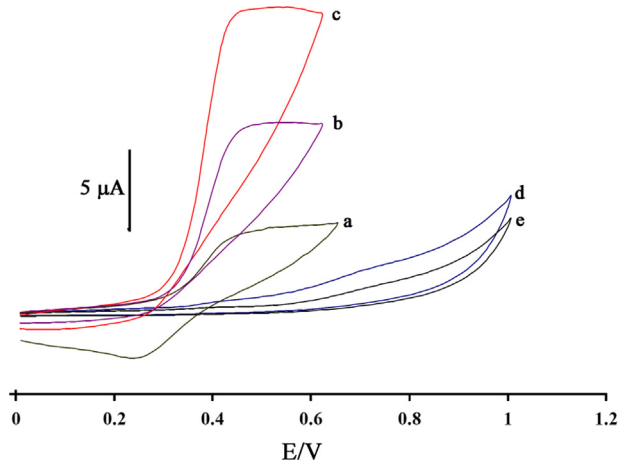

Fig. 2. Cyclic voltammograms of (a) the buffer solution at NHPDA/FePt/CNTs/CPE; (b) 300 μmol L^{-1} GSH at NHPDA/CPE; (c) 300 μmol L^{-1} GSH at NHPDA/FePt/CNTs/CPE; (d) 300 μmol L^{-1} GSH at FePt/CNTs/CPE and (e) 300 μmol L^{-1} GSH at CPE. Conditions: 0.1 mol L^{-1} PBS (pH 7.0), scan rate of 10 mV s^{-1}.

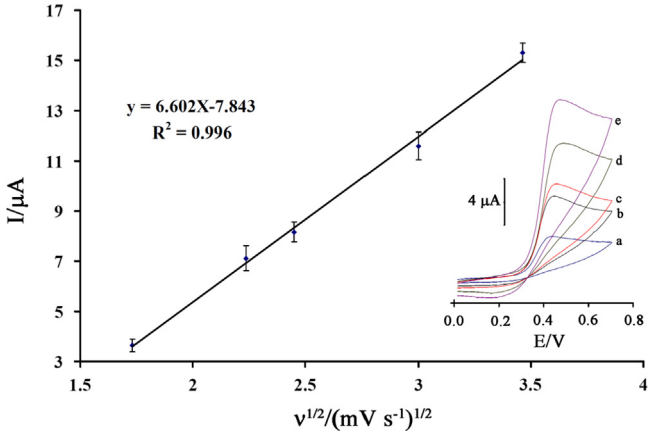

Fig. 3. Plot of I_{pa} vs. $\nu^{1/2}$ for the oxidation of GSH at NHPDA/FePt/CNTs/CPE. Inset: cyclic voltammograms of GSH at various scan rates: (a) 3 mV s^{-1}, (b) 5 mV s^{-1}, (c) 6 mV s^{-1}, (d) 9 mV s^{-1} and (e) 12 mV s^{-1} in 0.1 mol L^{-1} PBS (pH 7.0) (the error bars are standard deviations for $n=3$).

at NHPDA/CPE (curve *b*) was about 410 mV, while it was about 700 mV at FePt/CNTs/CPE (curve *d*). At the unmodified CPE, the peak potential of GSH was about 720 mV (curve *e*). From these results, it was concluded that the best electrocatalytic effect for GSH oxidation was the one observed at NHPDA/FePt/CNTs/CPE (curve *c*). For example, the results show that the peak potential of GSH oxidation at NHPDA/FePt/CNTs/CPE (curve *c*) shifted by about 200 mV and 220 mV toward negative values when compared to that at FePt/CNTs/CPE (curve *d*) and at CPE (curve *e*), respectively. Similarly, when comparing the oxidation of GSH to disulphide at NHPDA/FePt/CNTs/CPE (curve *c*) relative to that at NHPDA/CPE (curve *b*), a dramatic enhancement was observed in the anodic peak current at NHPDA/FePt/CNTs/CPE relative to that obtained at NHPDA/FePt/CNTs/CPE. In other words, the data clearly show that the combination of NHPDA and FePt/CNTs definitely improve the characteristics of GSH oxidation. This behavior is typical of that expected for electrocatalysis at chemically modified electrodes (Fig. S1 Supporting information) (Raoof et al., 2008; Karimi-Maleh et al., 2010).

The effect of scan rate (υ) on the oxidation current of GSH was also examined (Fig. 3 inset). The results showed that the peaks current increased linearly with increasing the square root of scan rate that ranged from 3 to 12 mV s^{-1} according to regression equation of: (Fig. 3)

$$I_p = 6.602\nu^{1/2} - 7.843 (r^2 = 0.996, I \text{ in } \mu A, \nu \text{ in mV s}^{-1}) \quad (1)$$

The result shows that the electrode process is controlled under the diffusion step. In addition, with increasing the potential scan rate, the catalytic oxidation peak potential gradually shifts towards more positive potentials, suggesting a kinetic limitation in the reaction between the redox site of the NHPDA and GSH.

In order to obtain information on the rate determining step, a Tafel plot was developed for NHPDA/FePt/CNTs/CPE using the data derived from the raising part of the current–voltage curve. The slope of the Tafel plot is equal to $n(1-\alpha)F/2.3RT$ which comes up to 0.117 V $decade^{-1}$. We obtained $n\alpha$ equal to 0.5. Assuming $n=1$, then $\alpha=0.5$. In addition, the value of αn_α (n_α is the number of electrons involved in the rate determining step) was calculated for the oxidation of GSH at pH 7.0 for both FePt/CNTs/CPE and NHPDA/FePt/CNTs/CPE using the following equation:

$$\alpha n_\alpha = 0.048/(E_P - E_{P/2}) \quad (2)$$

where, $E_{P/2}$ is the potential corresponding to $I_{P/2}$. The values for αn_α were found to be 0.18 and 0.51 at the surface of both FePt/CNTs/CPE and NHPDA/FePt/CNTs/CPE, respectively. These values show that the over-potential of GSH oxidation is reduced at the surface of NHPDA/FePt/CNTs/CPE, and also that the rate of electron transfer process is greatly enhanced. This phenomenon is, thus, confirmed by the larger I_{pa} values recorded during cyclic voltammetry at NHPDA/FePt/CNTs/CPE.

3.3. Chronoamperometric study

In continuous, the chronoamperometric behaviors of NHPDA/FePt/CNTs/CPE was examined both in the absence and in the presence of GSH by setting the working electrode potential at 0.1 V (at the first potential step) and 0.65 V (at the second potential step) vs. Ag|AgCl|KCl_{sat} (Fig. S2 Supporting information(A)). As can be seen, when the potential is stepped from 0.10 to 0.65 V vs. Ag|AgCl|KCl_{sat}, there is not net cathodic current corresponding to the reduction of the mediator in the presence of GSH. In the presence of GSH, however, the charge value associated with the forward chronoamperometry is significantly greater than that observed for the backward chronoamperometry. Fig. S2(B) supporting information shows the plots of currents sampled at a fixed time as a function of GSH concentration added to a blank solution (pH 7.0) at different times after the application of the potential step. Comparison of graphs (a)–(d) in this figure suggests that in all the cases, a consistent connection holds between the currents measured at a fixed time and GSH concentration, but the slope of the calibration graph increases with a decrease in the time elapsed after a potential-step is applied. The linearity of the electrocatalytic current vs. $t^{-1/2}$ indicates that the current must be controlled by diffusion of GSH from the bulk of the solution toward the surface of the electrode (Fig. S2 Supporting information(B)). Therefore, the slope of this linear plot can be used to estimate the diffusion coefficient, *D*, of GSH. The mean value of *D* was found to be 8.37×10^{-5} cm^2 s^{-1}. These results show that the mediator at the surface of NHPDA/FePt/CNTs/CPE can catalyze the oxidation of GSH.

Chronoamperometry can also be employed to evaluate the catalytic rate constant, *k*, for the reaction between GSH at the NHPDA/FePt/CNTs/CPE according to the method of Galus (1976)

$$I_C/I_L = \gamma^{1/2}[\pi^{1/2}\text{erf}(\gamma^{1/2}) + \exp(-\gamma)/\gamma^{1/2}] \quad (3)$$

where, I_C is the catalytic current of GSH at the surface of NHPDA/FePt/CNTs/CPE, I_L the limited current in the absence of GSH, and $\gamma = kC_b t$ (C_b is the bulk concentration of GSH) is the argument of the

error function. In cases where γ exceeds 2, the error function is almost equal to 1 and, therefore, the above equation can be reduced to

$$I_C/I_L = \pi^{1/2}\gamma^{1/2} = \pi^{1/2}(kC_b t)^{1/2} \quad (4)$$

where, t is the time elapsed (s). Eq. (4) can be used to calculate the rate constant of the catalytic process, k. Based on the slope of I_C/I_L vs. $t^{1/2}$ plot, k can be obtained for a given GSH concentration. The plots obtained from the chronoamperograms in Fig. S2(A) supporting information is presented in the same Fig. S2(C) supporting information. From the values of the slopes, an average value obtained for k is $k=5.81\times10^2\ M^{-1}\ s^{-1}$.

3.4. Electrochemical impedance spectroscopy

Electrochemical impedance spectroscopy was also employed to investigate the oxidation of GSH and PXM on NHPDA/FePt/CNTs/CPE. Fig. 4 presents Nyquist diagrams of the imaginary impedance (Z_{im}) vs. the real impedance (Z_{re}) of the EIS obtained at the modified electrode recorded at 0.38 V dc-offset in the absence (curve *a*) and in the presence of 300 μmol L^{-1} PXM (curve *b*), and 300 μmol L^{-1} GSH (curve *c*) in 0.10 mol L^{-1} PBS (pH 7.0), respectively. In the absence of GSH, the Nyquist diagram comprises a depressed semicircle at high frequencies which may be related to the combination of charge transfer resistance of NHPDA electrooxidation and the double-layer capacitance, followed by a straight line with a slope of nearly 45°. The latter is due to the occurrence of mass transport process via diffusion.

The equivalent circuit compatible with the Nyquist diagram recorded in the absence and presence of GSH is depicted in Fig. 4 inset. In this circuit, R_s, Q, and R_{ct} represent solution resistance, a constant phase element corresponding to the double-layer capacitance, and the charge transfer resistance associated with the oxidation of low-valence NHPDA species. W is a finite-length Warburg short-circuit term coupled to R_{ct}, which accounts for the Nernstian diffusion. In the presence of GSH, the diameter of the semicircle decreases, confirming the electrocatalytic capability of the mentioned electrocatalyst for oxidation of GSH. This is due to the instant chemical reaction of GSH with the high-valence NHPDA species. The catalytic reaction of oxidation of GSH that occurred via the participation of NHPDA species virtually caused an increase in the surface concentration of low valence species of electrocatalyst, and the charge transfer resistance declined, depending on the concentration of GSH in the solution. On the other hand, PXM could not be electrocatalyzed on this modified electrode to provide the necessary conditions for the selective determination of GSH in real samples.

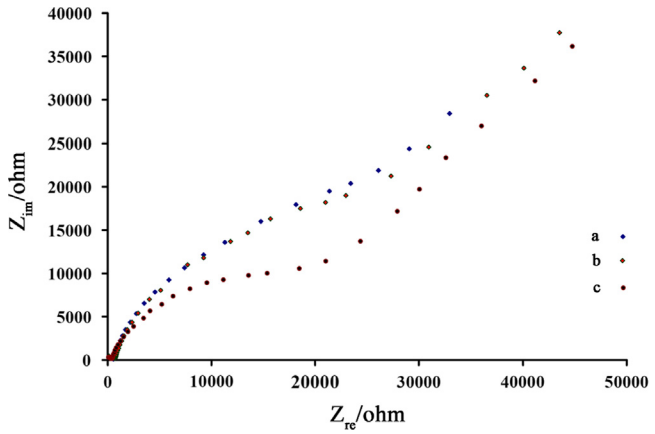

Fig. 4. Nyquist diagrams of NHPDA/FePt/CNTs/CPE (a) in the absence; (b) in the presence of 300 μmol L^{-1} PXM and (c) in the presence of 300 μmol L^{-1} GSH. Conditions: pH, 7.0; E_{DC}, +0.38 V vs. Ag/AgCl; E_{ac}, 5 mV; Frequency range, 100 kHz–0.1 Hz.

3.5. Simultaneous determination of GSH and PXM

Square wave voltammetry (with amplitude potential of 70 mV and frequency of 20 Hz) was used to determine GSH and PXM. SWVs clearly show that the plot of the peak current vs. GSH concentration is linear for 0.004–340 μmol L^{-1} of GSH, with a regression equation of $I_p(\mu A)=(0.168\pm0.023)C_{GSH}+(8.068\pm1.561)$ ($r^2=0.995$, $n=13$); while the regression equation for PXM in the range of 0.5–550 μmol L^{-1} is $I_p(\mu A)=(0.073\pm0.008)C_{PXM}+(0.763\pm0.825)$ ($r^2=0.998$, $n=9$), where C is μmol L^{-1} concentration of GSH and/or PXM, and I_p is the peak current. The detection limit (LOD) was 1.0 nmol L^{-1} GSH and 0.1 μmol L^{-1} PXM according to the definition of LOD$=3s_b/m$ (where S_b is the standard deviation of the blank signal ($n=8$) and m is the slope of the calibration. This value of detection limit, the linear dynamic range, and the sensitivity for GSH observed for the NHPDA/FePt/CNTs/CPE are comparable and even better than those obtained for several other modified electrodes (Table S1 Supporting information).

The main objective of this study was to measure GSH and PXM simultaneously. The effective application of the NHPDA/FePt/CNTs/CPE for this purpose was demonstrated by simultaneously changing GSH and PXM concentrations. Fig. 5A shows typical SWV for the simultaneous determination of GSH and PXM. Fig. 5B and C show the dependence of SWV peak currents on the concentration of GSH and PXM, respectively. The SW voltammetric results showed that simultaneous determination of GSH and PXM with two well-distinguished anodic peaks at 450 and 750 mV potentials, corresponding to the oxidation of GSH and PXM is possible at the modified electrode.

The sensitivity of the modified electrode towards the oxidation of GSH in the absence and presence of PXM were found to be 0.168 ± 0.023 and 0.167 ± 0.043 μA μM^{-1}, respectively. Also, the sensitivities of the modified electrode towards the oxidation of PXM in the absence and presence of GSH were found to be 0.073 ± 0.008 and 0.072 ± 0.009 μA μM^{-1}, respectively, which indicates that the oxidation processes of GSH and PXM at NHPDA/FePt/CNTs/CPE are independent and that the simultaneous or independent measurements of the two analytes are, therefore, possible without any interference.

3.6. Interference studies

The influence of various substances as potentially interfering compounds with the determination of GSH and PXM were studied under the optimum conditions with 4.0 μmol L^{-1} GSH and 125.0 μmol L^{-1} PXM at pH 7.0. The potentially interfering substances were chosen from the group of substances commonly found with GSH and PXM in pharmaceuticals and/or in biological fluids. The tolerance limit was defined as the maximum concentration of the interfering substance that caused an error less than ±5% for the determination of GSH and PXM. The results showed that 1000-fold of glucose, sucrose, lactose, fructose, methanol, and ethanol, 800-fold of K^+, Li^+, Na^+, Cl^-, Br^-, Ca^{2+}, Mg^{2+}, SO_4^{2-}, Al^{3+}, NH_4^+, and F^-, 500-fold of urea, 300-fold of histidine, glutamic acid, methionine, valine, glycine, phenylalanine and alanine, ascorbic acid (after addition of 0.1 mM ascorbic oxidaze) not affect the selectivity. Nor did saturation of starch solution interfere with the determination of GSH and PXM.

3.7. Stability and reproducibility

The reproducibility and stability of NHPDA/FePt/CNTs/CPE was investigated by SWV measurements of 5.0 μmol L^{-1} GSH. The results

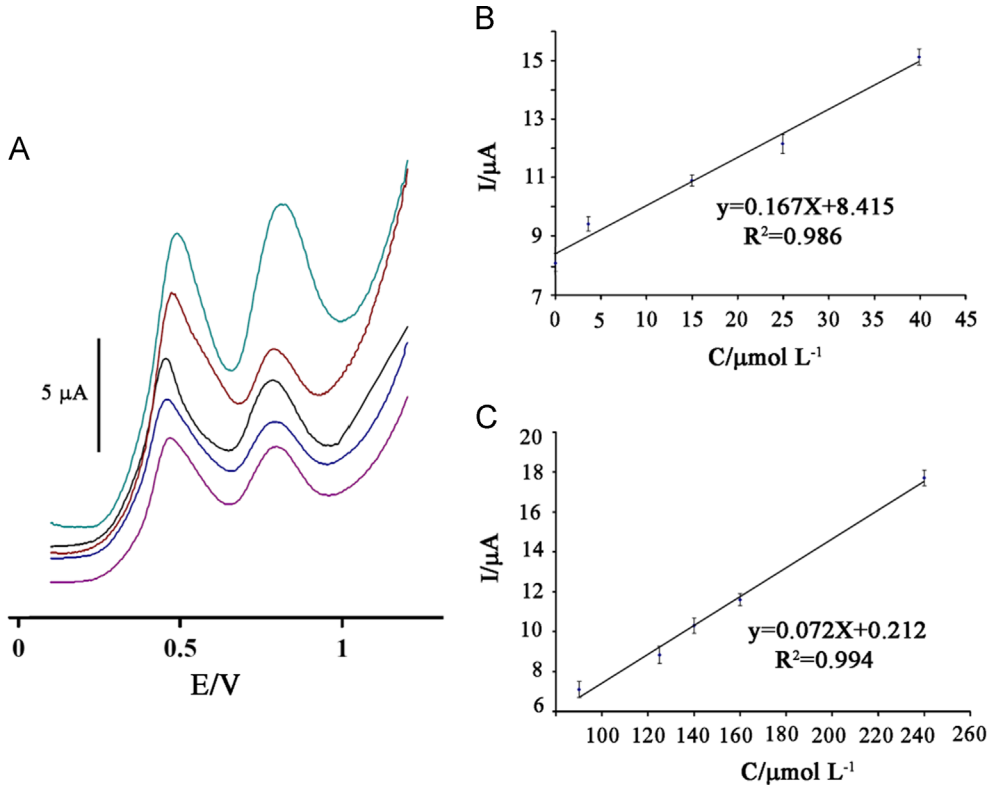

Fig. 5. (A) SWVs of NHPDA/FePt/CNTs/CPE in 0.1 mol L^{-1} PBS (pH 7.0) containing different concentrations of GSH–PXM in μmol L^{-1} (from inner to outer): 0.004+90.0; 3.6+125.0; 15.0+140.0; 25.0+160.0 and 40.0+240.0; respectively. Insets: Plots of I_p vs. (B) GSH and (C) PXM (the error bars are standard deviations for $n=3$).

Table 1
Determination of GSH and PXM in real samples ($n=3$).

Sample	GSH added	PXM added	Found (GSH) proposed method	Found (GSH) published method [34]	Found (PXM) proposed method	Found (PXM) published method [42]
Hemolyzed erythrocyte	–	–	5.2 ± 0.5	5.3 ± 0.6	–	–
	4.8	–	10.11 ± 0.4	10.5 ± 0.6	–	–
Tablet	20.0	–	19.78 ± 0.65	20.11 ± 0.75	–	–
	30.0	–	30.11 ± 0.75	30.94 ± 1.11	–	–
Urine	–	–	< LOD	< LOD	< LOD	< LOD
	3.5	25.0	2.11 ± 0.08	3.21 ± 0.55	24.65 ± 1.22	25.74 ± 1.15

All the '±' values are RSD% ($n=3$); *Concentration in the hemolysed erythrocyte reported in mmol L^{-1} and for urine and tablet samples in μmol L^{-1}.

showed that the relative standard deviation (RSD%) for seven successive assays was 1.5%. In addition, the repeatability of the prepared modified electrode was checked using four different electrodes for the analysis of 5.0 μmol L^{-1} GSH, using SWV. The results showed a RSD% of 2.8%. Moreover, the stability of the modified electrode was examined by storing of the electrode in the lab at room temperature. Then, the electrode was used for the analysis of 5.0 μmol L^{-1} GSH using SWV. The results showed that the electrode signal retained to 95% of its initial response after two week and 90% of its initial response after 45 days. These results indicate that NHPDA/FePt/CNTs/CPE has good stability and reproducibility, and could be used for GSH measurements up to five week.

3.8. Determination of GSH and PXM in real samples

In order to demonstrate the ability of the modified electrode to determine GSH and PXM in real samples, these compounds were determined in tablet and urine samples. The results are presented in Table 1. Clearly, NHPDA/FePt/CNTs/CPE is capable of voltammetric determination of GSH and PXM with high selectivity and good reproducibility.

4. Conclusion

In the present study, carbon-paste electrode modified with NHPDA and FePt/CNTs was used for the determination of GSH in the presence of PXM. The results show that the oxidation of GSH is catalyzed at pH 7.0, whereas the peak potential of GSH is shifted by 220 mV to a less positive potential at the surface of the NHPDA/FePt/CNTs/CPE. Potential difference of 300 mV between GSH and PMX was detected, which was large enough to determine GSH and PXM individually and simultaneously. Finally, the proposed sensor was successfully applied for the determination of GSH in pharmaceutical and biological samples.

Acknowledgements

The authors wish to thank Graduate University of Advanced Technology, Kerman, Iran, for their support.

Appendix A. Supporting information

Supplementary data associated with this article can be found in the online version at http://dx.doi.org/10.1016/j.bios.2014.03.055.

References

Bavili Tabrizi, A., 2007. J. Food Drug Anal. 15, 242–248.
Causse, E., Malatray, P., Calaf, R., Chariots, P., Candito, M., Bayle, C., Valdiguie, P., Salvayre, C., Couderc, F., 2000. Electrophoresis 21, 2074–2079.
Damiani, P.C., Bearzotti, M., Cabezón, M., Olivieri, A.C., 1998. J. Pharm. Biomed. Anal. 17, 233–236.
El-Sherbiny, G.A., Taye, A., Abdel-Raheem, I.T., 2009. Ann. Hepatol. 8, 134–140.
Ellman, G.L., 1959. Arch. Biochem. Biophys. 82, 70–77.
Elyasi, M., Khalilzadeh, M.A., Karimi-Maleh, H., 2013. Food Chem. 141, 4311–4317.
Ensafi, A.A., Khayamian, T., Hasanpour, F., 2008. J. Pharm. Biomed. Anal. 48, 140–144.
Ensafi, A.A., Dadkhah-Tehrani, S., Karimi-Maleh, H., 2012. Drug Test. Anal. 4, 978–985.
Ensafi, A.A., Taei, M., Khayamian, T., Karimi-Maleh, H., Hasanpour, F., 2010. J. Solid State Electrochem. 14, 1415–1423.
Ensafi, A.A., Karimi-Maleh, H., Ghiaci, M., Arshadi, M., 2011a. J. Mater. Chem. 21, 15022–15030.
Ensafi, A.A., Karimi-Maleh, H., Mallakpour, S., Rezaei, B., 2011b. Colloids Surf., B 87, 480–488.
Ensafi, A.A., Karimi-Maleh, H., Mallakpour, S., Hatami, M., 2011c. Sens. Actuators, B 155, 464–472.
Galus, Z., 1976. Fundamentals of Electrochemical Analysis. Ellis Horwood, New York.
Gupta, V.K., Atar, N., Yola, M.L., Üstündağ, Z., Uzun, L., 2014. Water Res. 48, 210–217.
Gupta, V.K., Chandra, S., Lang, H., 2005. Talanta 66, 575–580.
Gupta, V.K., Yola, M.L., Atar, N., Solak, A.O., Uzun, L., Üstündağ, Z., 2013. Electrochim. Acta 105, 149–156.
Kamata, K., Takahashi, M., Terajima, K., Nishijima, M., 1995. Analyst 120 (2755-2258).
Kandar, R., Zakova, P., Lotkova, H., Kucera, O., Cervinkova, Z., 2007. J. Pharm. Biomed. Anal. 43, 1382–1387.
Karimi-Maleh, H., Biparva, P., Hatami, M., 2013. Biosens. Bioelectron. 48, 270–275.
Karimi-Maleh, H., Ensafi, A.A., Allafchian, A.R., 2010. J. Solid State Electrochem. 14, 9–15.
Katrusiak, A.E., Paterson, P.G., Kamencic, H., 2001. J. Chromatogr. B 758, 207–212.
Keyvanfard, M., Karimi-Maleh, H., Alizad, K., 2013. Chin. J. Catal. 34, 1883–1889.
Liang, S.C., Wang, H., Zhang, Z.M., Zhang, X., Zhang, H.S., 2002. Anal. Chim. Acta 451, 211–219.
Micheli, L., Fiaschi, A.I., Cerretani, D., Giorgi, G., 1993. Ann. Ist. Super. Sanita. 29, 387–390.
Moradi, R., Sebt, S.A., Karimi-Maleh, H., Sadeghi, R., Karimi, F., Bahari, A., Arabi, H., 2013. Phys. Chem. Chem. Phys. 5, 5888–5897.
Nagendra, P., Yathirajan, H.S., Rangappa, K.S., 2002. J. Indian Chem. Soc. 79, 602.
Rabenstein, D.L., Brown, D.W., McNeil, C.J., 1985. Anal. Chem. 57, 2294–2299.
Raggi, M., Nobile, L., Giovannini, A.G., 1991. J. Pharm. Biomed. Anal. 9, 1037–1040.
Raoof, J.B., Ojani, R., Karimi-Maleh, H., 2009a. J. Appl. Electrochem. 39, 1169–1175.
Raoof, J.B., Ojani, R., Kolbadinezhad, M., 2009b. J. Solid State Electrochem. 13, 1411–1416.
Raoof, J.B., Ojani, R., Karimi-Maleh, H., 2008. Electroanalysis 20, 1259–1262.
Sanghavi, B.J., Srivastava, A.K., 2011. Electrochim. Acta 56, 4188–4196.
Sanghavi, B.J., Sitaula, S., Griep, M.H., Karna, S.P., Ali, M.F., Swami, N.S., 2013. Anal. Chem. 85, 8158–8165.
Sanghavi, B.J., Srivastava, A.K., 2010. Electrochim. Acta 55, 8638–8648.
Sanati, A.L., Karimi-Maleh, H., Badiei, A., Biparva, P., Ensafi, A.A., 2014. Mater. Sci. Eng., C 35, 379–385.
Satoh, I., Arakawa, S., Okamoto, A., 1988. Anal. Chim. Acta 214, 415–419.
Xu, F., Wang, L., Gao, M., Jin, L., Jin, J., 2002. Anal. Bioanal. Chem. 372, 791–794.
Yola, L.M., Atar, N., Üstündağ, Z., Solak, A.O., 2013. J. Electroanal. Chem. 698, 9–16.
Yola, M.L., Atar, N., Qureshi, M.S., Üstündağ, Z., Solak, A.O., 2012. Sens. Actuators, B 171–172, 1207–1215.
Zhang, J.Y., Hu, Z.D., Chen, X.G., 2005. Talanta 65, 986–990.